Nature of the N−H···S Hydrogen Bond

Himansu S. Biswal[†] **and Sanjay Wategaonkar***

Department of Chemical Sciences, Tata Institute of Fundamental Research, Homi Bhabha Road, Colaba, Mumbai 400 005

Received: August 8, 2009; Revised Manuscript Received: August 28, 2009

The N−H···S hydrogen-bonded complexes of the model compounds of tryptophan (indole and 3-methylindole) and methionine (dimethyl sulfide, Me_2S) have been characterized by a combination of experimental techniques like resonant two-photon ionization (R2PI), resonant ion dip infrared spectroscopy (RIDIRS), and fluorescence dip infrared spectroscopy (FDIRS) and computational methods like ab initio electronic structure calculations, atoms-in-molecules (AIM), natural bond orbital (NBO), and energy decomposition analyses. The results are compared with the N−H···O (M·H_2O; M = indole, 3-methyl indole) σ-type and N−H···Φ (M·benzene) π-type hydrogen-bonded complexes. It was shown that the S_1-S_0 band origin red shifts in the N−H···S hydrogen-bonded complexes correlated well with the polarizability of the acceptor rather than their proton affinity, contrary to the trend observed in most X−H···Y (X, Y = O, N, halogens, etc.) hydrogen-bonded systems. The red shift in the N−H stretching frequency in the N−H···S HB clusters (Me_2S as HB acceptor) was found to be 1.8 times greater than that for the N−H···O hydrogen-bonded complexes (H_2O as HB acceptor), although the binding energies for the two complexes were comparable. The energy decomposition analyses for all of the N−H···S hydrogen-bonded complexes showed that the correlation (or dispersion) energy has significant contribution to the total binding energy. It is pointed out that the binding energy of the N−H···S complex was also comparable to that of the indole·benzene complex, which is completely dominated by the dispersion interaction. Atoms-in-molcules (AIM) and natural bond orbital (NBO) analyses indicated a nontrivial electrostatic component in the hydrogen-bonding interaction. Greater dispersion contribution to the stabilization energy as well as greater red shifts in the N−H stretch relative to those of N−H···O hydrogen-bonded complexes makes the indole·dimethylsulfide complex unique in regard to the simultaneous influence of both the dispersion and electrostatic forces. For the sake of comparison, it is pointed out that the red shifts in the O−H stretch for O−H···S and O−H···O hydrogen-bonded complexes were almost the same in the case of *para*-cresol·Me_2S and *para*-cresol·H_2O complexes (*J. Chem. Phys.* **2008**, *128*, 184311. and *J. Phys. Chem. A* **2009**, *113*, 5633−5643). This suggests that the strength of the N−H···S hydrogen bonding is stronger than the N−H···O hydrogen bonding. The N−H···S hydrogen bonding was observed for the first time using jet-cooled conditions, and the most interesting feature of this study is that N−H···S "σ-type" hydrogen bonding behaves more like C−H···Φ or N−H···Φ "π-type" hydrogen bonding in regard to the dispersion domination in the total interaction energy.

1. Introduction

Although the concept of the hydrogen bond is almost a century old,[1] it is still evolving because of the novel experimental findings and high-level computational results.[2] This is the single most important noncovalent interaction, which plays a crucial role in governing the physical and chemical properties of the solvents, controls solute−solvent interactions, and most importantly provides a specific shape, stability, and functionality to the biomolecules like proteins and DNA. The commonly observed hydrogen bonds involve the first row elements such as N, O, and F, and these are most extensively studied and well characterized. The nature of the interaction in these cases is electrostatic in origin, which is responsible for their directionality. The hydrogen-bonding interactions involving the second row elements such as P, S, and Cl are not any less abundant.[3] However, investigations of these are very sparse due to various reasons, namely, they are less electronegative compared to the first row elements, and there is poorer match between the hard proton (hard acid) and soft bases like P, S, and so forth. It would be very interesting to look at the properties, origin, and strength of X−H···Y hydrogen bonds involving the X and/or Y atoms belonging to the second row elements. As a first step in this direction, we have investigated the X−H···S HBs, where X is O or N. Sulfur is the choice replacement for Y as almost all living systems contain several important sulfur-containing molecules, including two amino acids, methionine and cysteine.

Our first report on the O−H···S HB in the model compounds of tyrosine and methionine[4] followed by the comprehensive study of O−H···O versus O−H···S HB in the *p*-cresol−H_2O/H_2S complexes revealed that the O−H···S HB is relatively weaker and predominantly dispersive in nature.[5] In this work, we have investigated the N−H···S type HB in the model compounds of tryptophan and methionine. The existence of N−H···S HB is evident from the crystal structure data for β-lactam antibiotics such as pencillins,[6] the active site of proteins like cytochrome-P450 and nitric oxide synthase,[7−9] the iron−sulfur proteins,[10−13] as well as in the organic crystals.[14−18] However, the microscopic data on the N−H···S HB is nonexistent in the literature. Owing to the importance of the N−H···S HB in the

* To whom correspondence should be addressed. Phone: 91-22-2278-2259. Fax: 91-22-2278-2106. E-mail: sanwat@tifr.res.in.
† E-mail: himansu@tifr.res.in.

10.1021/jp907658w CCC: $40.75
Published on Web 10/15/2009

aforementioned systems, a greater understanding of this interaction at the molecular level is essential. This in turn may provide better insight into the understanding of the protein folding and biochemical reactions involving the formation and rupture of N−H···S HB, and so forth. Keeping in mind its importance in the biological systems, the obvious choice for the HB donor was indole and substituted indole (model for the amino acid tryptophan),[19] and that for the HB acceptor was the dimethyl sulfide (model compound for the amino acid methionine side chain).[4]

Indole is an aromatic chromophore responsible for the fluorescence of a naturally occurring amino acid, tryptophan. It is a well-established model compound for tryptophan and has been extensively used to probe the local environment and dynamics of proteins in different solvents.[19−25] It is known that the photophysical properties of indole, such as the fluorescence quantum yield, radiative lifetime, and so forth, are very sensitive to local environment. In fact, a lot of experimental investigations have been performed on the isolated indole and its complexes with different solvent molecules like H_2O, MeOH, and NH_3.[26−39] The N−H···X type hydrogen-bonded complexes (where X = O or N) are well studied ones, and these are largely electrostatic in nature.

In this work, we have used laser spectroscopy in conjunction with the supersonic jet expansion technique to investigate the indole−dimethylsulfide complexes, and ab intio calculations were used to explore the nature of the N−H···S hydrogen bond. The objective of this work is to characterize N−H···S HB and compare it with the N−H···O HB (indole·water complex) in these model compounds. From the results, it is evident that N−H···S is quite different from all other complexes that have been reported so far. While it shows greater red shift in the N−H stretching frequency compared to that in the case of the N−H···O HB complex, which is an indicator of a stronger H-bond, the computed binding energy is almost comparable or only slightly greater than that of the N−H···O complex. The dispersion contribution turns out to be the major attractive interaction as that observed in the case of indole·benzene complex reported by Braun et al.[34] In the case of the indole·benzene complex, complexity arises in assigning the structure unequivocally as there are two possibilities, namely, the π-stacked complex and the N−H···Φ π-type hydrogen-bonded complex. Braun et al.,[34] using MATI spectroscopy and computational studies, gave indirect evidence of the N−H···Φ hydrogen-bonded complex. In the present work, we investigated the indole·benzene complex using FDIR spectroscopy, and the results support the N−H···Φ π-type of interaction reported by Braun et al. The basic difference between the N−H···X σ-type and N−H···Φ π-type hydrogen-bonded complexes is that the σ-types are electrostatic in nature while the π-types are dispersive in nature. In this context, it is important to note that our findings suggest that the N−H···S interaction compares well with the N−H···Φ π-type hydrogen-bonded complex in regard to the nature of interaction and the binding energy rather than the N−H···X σ-type interaction.

2. Experimental Details

The hydrogen-bonded complexes have been investigated experimentally using resonant two-photon ionization (R2PI), resonant ion dip infrared spectroscopy (RIDIRS), and fluorescence dip infrared spectroscopy (FDIRS). The experimental setup has been described in more detail elsewhere.[40] The complexes were produced in a pulsed supersonic expansion with helium as the carrier gas. The experimental setup consisted of two 10 in. diameter differentially pumped stainless steel chambers. A 500 μm pulsed nozzle (General Valve, series 9) housed in the first chamber was used to generate a cold beam of molecules, which was collimated using a skimmer located ∼25 mm downstream from the nozzle orifice. The monomers and the hydrogen-bonded complexes were ionized by frequency-doubled dye lasers via the two-color-R2PI (2c-R2PI) technique. For the 2c-R2PI experiments, a 10 Hz, nanosecond Nd^{3+}:YAG (Quantel Brilliant) pumped dye laser (Molectron DL18P) was used to provide the fixed D_0-S_1 ionization source, and another Nd^{3+}:YAG (Quantel YG781C) laser pumped dye laser (Quantel TDL70) was used to provide the tunable S_1-S_0 excitation source. The two copropagating beams were spatially and temporally overlapped and were focused onto the molecular beam using a 50 cm focal length lens. Typical pulse energies were ∼5−10 μJ for the excitation laser and ∼100 μJ for the ionization laser. The ions were mass analyzed in a linear time-of-flight mass spectrometer (TOFMS) with a 50 cm flight tube and detected by a 25 mm diameter channeltron multiplier (Dr. Sjuts Optotechnik GmbH; KBL25RS) housed in the second chamber. The output of the channeltron was sent to a digital storage oscilloscope (LeCroy 9450) interfaced to a PC through a preamplifier (ORTEC, Model VT120) via a GPIB port. The dye lasers were calibrated by means of the optogalvanic method using a Fe−Ne hollow cathode lamp.

Resonance ion dip infrared spectroscopy (RIDIRS) and FDIRS were used to record the IR spectra of the indole, 3-methylindole, and their complexes. In the RIDIRS technique, the S_1-S_0 electronic excitation laser was tuned to the band origin transition of a particular species, and the ionization laser was set a little above the D_0-S_1 transition, which made the ion signal proportional to the ground-state population of the species in the beam. The tunable IR laser was introduced 50−100 ns prior to the UV laser pulse. Whenever the IR laser is resonant with the vibrational transition of the species being probed, it depletes the population of the species in the ground state. The infrared resonances were detected as the dips in the ion signal because of the population depletion. The tunable IR source was a ∼10 ns, 10 Hz seeded Nd^{3+}:YAG laser (Quanta-Ray PRO Series, PRO 230-10) pumped dye laser (Sirah, CSTR LG 18). The dye laser output was mixed with the 1064 nm output of the Nd^{3+}:YAG laser in a $LiNbO_3$ crystal to generate the IR output by the difference frequency generation technique. The O−H and N−H stretching regions were covered using styryl-8 dye (Exciton, Inc.), while the C−H stretch region was covered by styryl-9 dye. All three lasers were temporally synchronized by a master controller (SRS DG-535). The FDIRS technique is similar to the RIDIRS, except that one probes the S_1-S_0 fluorescence intensity instead of the ion signal.

The reagents indole, 3-methylindole, and dimethylsulfide were purchased from Sigma−Aldrich and used without further purification. The reagents were heated to about 60−80 °C to generate sufficient vapor pressure to record the spectra with a good *S/N* ratio. A 2−5% premix of Me_2S in helium was used to generate a 1:1 complex of M·Me_2S complexes. Helium obtained from local commercial sources was used without further purification as the buffer gas. The buffer gas was flowed over a reagent bottle containing H_2O to synthesize the M·H_2O complexes. The optimum amount of H_2O vapors required for generating the 1:1 complex was maintained by means of a needle valve. The typical backing pressure employed during the experiments was 2.5−3 atm. The typical working pressure in the source chamber was $\sim 6 \times 10^{-5}$ Torr, and in the TOFMS chamber, it was $\sim 2 \times 10^{-6}$ Torr.

3. Computational Details

The Gaussian03 program suite[41] was used for the ab initio molecular orbital calculations to evaluate total interaction energies. The geometrical parameters of all of the complexes and the related free monomers were fully optimized at the MP2/aug-cc-pVDZ and B3LYP/aug-cc-pVDZ levels of theory. The equilibrium structures were examined by the harmonic vibrational frequency calculations at both levels of theory. The interaction energies for all of the complexes were calculated after applying the zero-point energy (ZPE), the basis set superposition error (BSSE), and the fragment relaxation energy corrections to the total binding energy. The MP2 level interaction energies were calculated using aug-cc-pVXZ (X = D and T) basis sets. The MP2 interaction energies at the basis set limit were estimated using the two-point extrapolation formula of Helgaker et al.[42] The three-dimensional pictures of the complexes were generated using ChemCraft graphics program (trial version).[43]

The theory of atoms-in-molecules (AIM)[44−46] was used to investigate the electronic densities and the intermolecular hydrogen-bonding interactions. The topological properties of electron densities for the monomers and complexes at the bond critical points (BCPs) were calculated using the AIM2000 program.[47] The wave functions computed at the MP2/aug-cc-pVDZ level of theory were used to calculate the electron density $\rho(r)$ and Laplacian $\nabla^2\rho(r)$ at the bond critical points and the integrated properties like atomic charge q(H), atomic polarization moment M(H), atomic volume v(H), and atomic energy E(H) in the atomic basin of hydrogen. To evaluate the direction and magnitude of the donor−acceptor interactions, the natural bond orbital (NBO)[48−50] analysis for all of the complexes was performed using the NBO 5.0 program.[51]

The interaction energies of the complexes were decomposed into physically meaningful individual energy components[52] at the HF/aug-cc-pVDZ level of theory using the natural energy decomposition analysis (NEDA),[53−55] Kitaura and Morokuma (KM),[56] and reduced variational space self-consistent field (RVS)[57] decomposition analyses. The KM and RVS decomposition analyses were performed using the Gordon and Chen[58] algorithm in GAMESS, U.S.A.[59] NEDA calculations were performed with the NBO 5.0 program[49,51] linked to the GAMESS package.

4. Experimental Results

Figure 1 displays the 2c-R2PI spectra of indole (IND) and its complexes with H_2O and Me_2S. In all cases, the ionization laser energy was kept at 27778 cm^{-1}. The $S_1 \leftarrow S_0$ electronic origins of IND, IND·H_2O, and IND·Me_2S were observed at 35241, 35109, and 35071 cm^{-1}, respectively. The observed spectral features for the monomer and its water complex were in good agreement with the reported spectra.[30,33,60,61] The red shift in the band origin of the IND·Me_2S complex was 170 cm^{-1}, whereas that for the water complex was 132 cm^{-1}. The indole monomer exhibited very little Franck−Condon (FC) activity in the R2PI spectrum, and this aspect was not any different in its H_2O and Me_2S complexes. A small peak appeared at 30 cm^{-1} toward blue side of the band origin for the water complex, whereas for its Me_2S complex, there was a fairly strong peak at 15 cm^{-1} from the band origin. These features were attributed to the intermolecular low-frequency normal modes.

Figure 2 displays the 2c-R2PI spectra of 3-methylindole (3-MI) and its complexes with H_2O and Me_2S. The positions of the band origins of 3-MI and its water and Me_2S complexes were observed at 34882, 34643, and 34624 cm^{-1}, respectively.

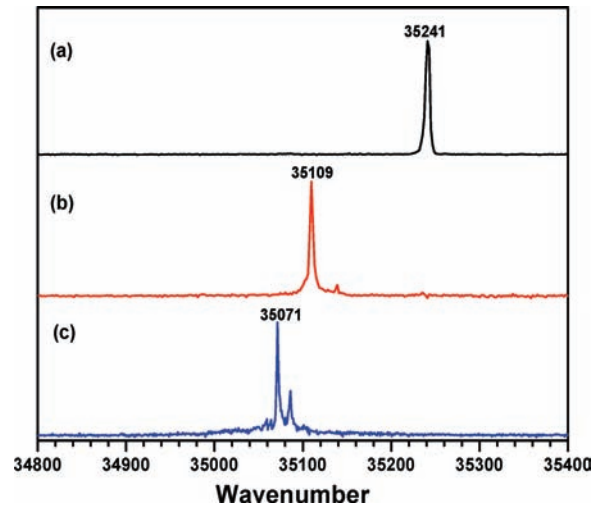

Figure 1. Two-color R2PI spectra of (a) indole, (b) IND·H_2O, and (c) IND·Me_2S.

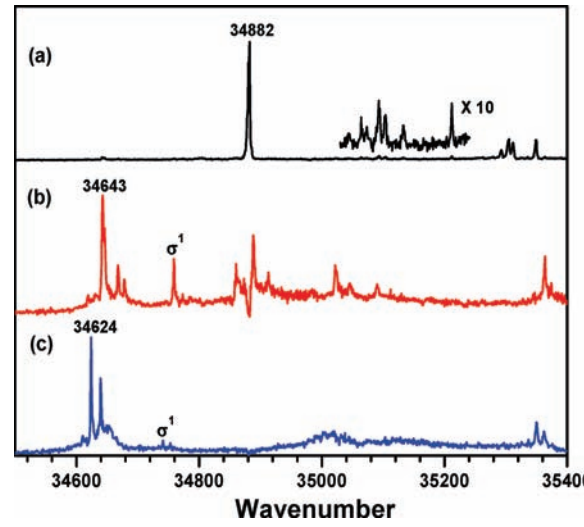

Figure 2. Two-color R2PI spectra of (a) 3-methylindole, (b) 3-MI·H_2O, and (c) 3-MI·Me_2S.

The observed spectral features for the monomer and its water complex are in good agreement with the reported spectra.[30,33] The red shift in the band origin of the 3-MI·Me_2S complex was 258 cm^{-1}, whereas that of its water complex was 239 cm^{-1}. The red shifts in the band origins of IND·Me_2S and 3-MI·Me_2S complexes are larger compared to those of their respective H_2O complexes, although the relative increase in the case of 3MI·Me_2S complex was smaller. The FC activity in the R2PI spectra of both the complexes of 3-MI was substantially greater than that observed in case of the monomer. The FC activity in the region of 35100 cm^{-1} of the monomer had increased 10-fold in the corresponding region (~34900 cm^{-1}) of the H_2O complex. The dip in the 3-MI·H_2O spectrum at 34882 cm^{-1} is due to the detector saturation by the monomer signal at this position. A feature observed at 34758 cm^{-1} was ascribed to the intermolecular H-bond stretching mode giving the stretching frequency as 115 cm^{-1}. A couple of features were also observed within 20 cm^{-1} of the band origin. In the 3-MI·Me_2S complex, the sharp features in the 34900 cm^{-1} region were replaced by a broad hump which was shifted by about 100 cm^{-1} toward the blue side. A weak feature at 34741 cm^{-1} was assigned to the H-bond stretching frequency (σ = 117 cm^{-1}).

The FDIR spectra for the IND and 3-MI monomers and their complexes in the N−H stretching frequency range are shown

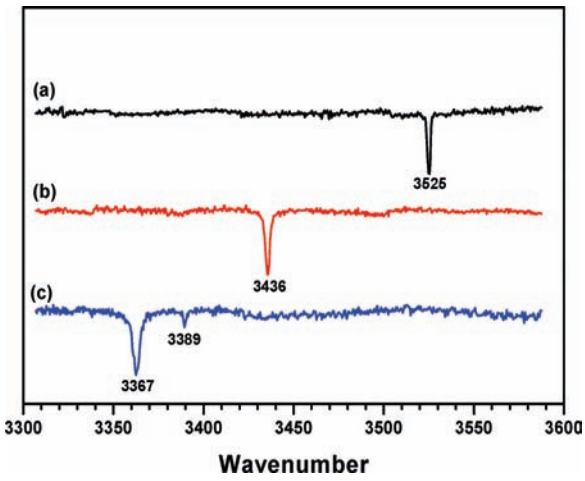

Figure 3. FDIR spectra of (a) indole, (b) IND·H_2O, and (c) IND·Me_2S in the N−H stretch region, recorded while tuning the probe laser at the band origin of the respective species.

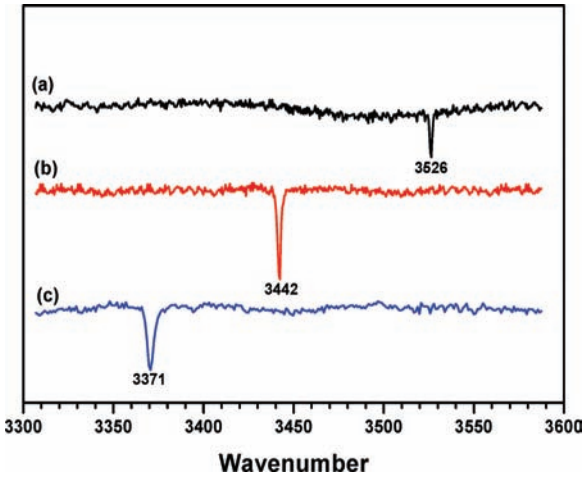

Figure 4. FDIR spectra of (a) 3-methylindole, (b) 3-MI·H_2O, and (c) 3-MI·Me_2S in the N−H stretch region, recorded while tuning the probe laser at the band origin of the respective species.

in Figures 3 and 4, respectively. The N−H stretch for IND·H_2O and IND·Me_2S appeared at 3436 and 3367 cm^{-1} and were red shifted by 89 and 158 cm^{-1}, respectively, with respect to that of indole. Similarly, the red shift in the N−H stretch of the 3-MI·H_2O complex was 84 cm^{-1} and that for the 3-MI·Me_2S complex was 154 cm^{-1}. If one goes by the conventional wisdom about correlation between the red shift in the X−H stretching frequency and the strength of the hydrogen bond, then it can be inferred that the N−H···S is significantly stronger than the N−H···O HB, giving rise to almost two times greater red shift for the N−H···S complex. Computational results show that three different conformers of M·Me_2S (M = IND or 3-MI) complexes exist within the energy difference of 1 kcal/mol from each other, vide infra. These conformers differ from each other by the orientation of two methyl groups of Me_2S, that is, they are either oriented toward the phenyl side [M·Me_2S (ph)] or pyrrole side [M·Me_2S (py)] or are perpendicular to the plane of the indole molecule [M·Me_2S (⊥)]. However, the IR−UV hole-burning spectra indicates the presence of only one conformer.

Figure 5 shows the FDIR spectra in the C−H stretch region for the IND and its complexes with H_2O (Figure 5b) and Me_2S (Figure 5c), while those for 3-MI and its complexes are presented in Figure 6. On the basis of the positions and relative intensities in computed IR spectra at the MP2/aug-cc-pVDZ level, it was inferred that the peaks labeled I to III in Figure 5

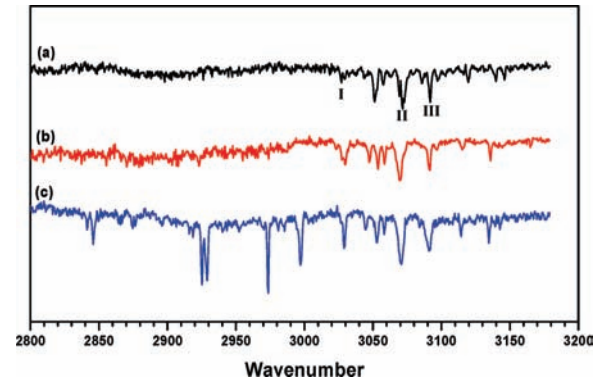

Figure 5. FDIR spectra of (a) indole, (b) IND·H_2O, and (c) IND·Me_2S in the C−H stretch region, recorded while tuning the probe laser at the band origin of the respective species.

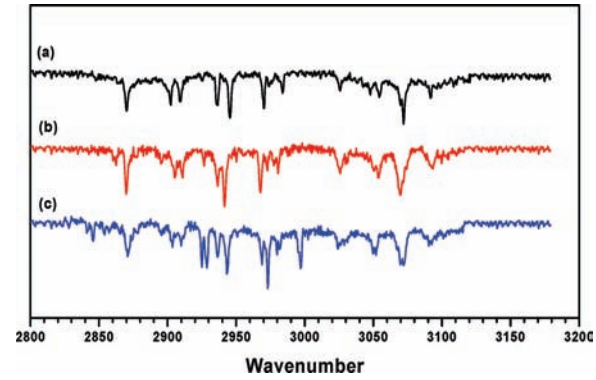

Figure 6. FDIR spectra of (a) 3-methylindole, (b) 3-MI·H_2O, and (c) 3-MI·Me_2S in the C−H stretch region, recorded while tuning the probe laser at the band origin of the respective species.

were the phenyl CH stretches and the features appearing between peaks I and II were some combination bands. The pyrrole CH stretches could only be observed in the case of indole. For both the IND·L and the 3-MI·L (L = ligand such as H_2O and Me_2S) complexes, the phenyl C−H stretches were broadened, and the IR spectrum for the Me_2S complex was remarkably similar to that of the H_2O complex in this region. The methyl C−H stretches of Me_2S at 2925, 2929, and 2975 cm^{-1} were blue shifted up to ~6 cm^{-1} compared to the corresponding monomer C−H stretches.[62]

5. Computational Results

5.1. Equilibrium Geometry and Interaction Energy. The geometry optimization for the monomers and their complexes was done at the DFT level using the B3LYP hybrid functional and at the MP2 level of theory with the aug-cc-pVDZ basis set followed by the frequency calculations to ensure that all of the structures were the true minima. Three different initial structures were generated by changing the orientation of Me_2S along the N−H···S axis. These conformers differ from each other by the orientation of two methyl groups of Me_2S, that is, they are either oriented toward the phenyl side [M·Me_2S (ph)] or pyrrole side [M·Me_2S (py)] or are perpendicular to the plane of the indole molecule [M·Me_2S (⊥)]. Figure 7 shows the initial and final geometries of the conformers optimized at the B3LYP and MP2 levels of theory. Three conformers were obtained at the MP2 level, but only two conformers were seen at the B3LYP level. The M·Me_2S (⊥) conformers optimized at the MP2 level did not show any N−H···S HB interaction. The frequency calculations on M·Me_2S (⊥) complexes gave rise to one imaginary frequency, which suggest that these are not true minima.

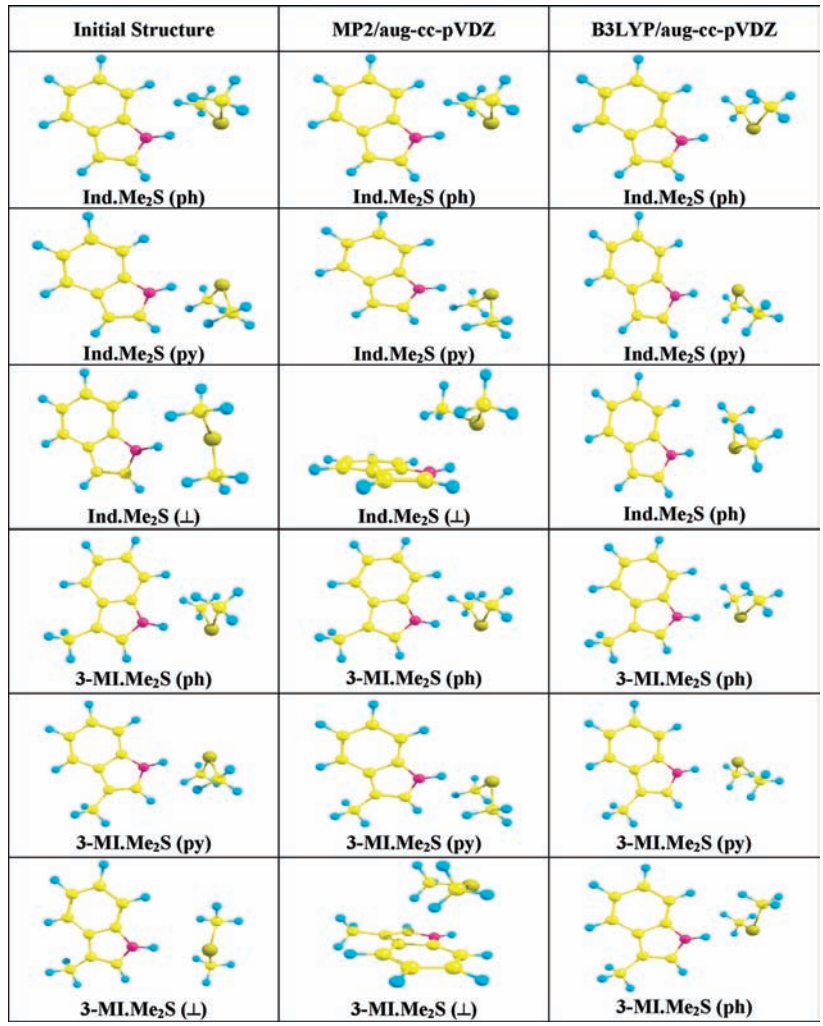

Figure 7. The stable structures of IND·Me_2S and 3-MI·Me_2S obtained at the MP2/aug-cc-pVDZ and B3LYP/aug-cc-pVDZ levels.

TABLE 1: Ab Initio Calculated Structural Parameters of IND·L and 3-MI·L Complexes (L = H_2O, H_2S, Me_2O, and Me_2S) at the MP2/aug-cc-pVDZ Level of Theory

	indole·L					3-methylindole·L				
geometrical parameters	H_2O	H_2S	Me_2O	Me_2S(ph)	Me_2S(py)	H_2O	H_2S	Me_2O	Me_2S(ph)	Me_2S(py)
$d_{H\cdots Y}$ (Å)	1.943	2.541	1.858	2.314	2.335	1.949	2.545	1.868	2.319	2.342
$R_{N\cdots Y}$ (Å)	2.962	3.507	2.864	3.327	3.331	2.967	3.506	2.868	3.331	3.335
Δr_{N-H} (Å)	0.007	0.005	0.012	0.012	0.011	0.007	0.005	0.012	0.011	0.011
θ (deg)	178.3	158.4	166.3	170.0	164.1	178.1	157.6	164.6	170.1	163.3
ψ (deg)	155.3	91.6	128.1	83.0	83.8	153.3	90.9	127.3	81.9	83.2

Therefore, henceforth, this structure will not be considered for any further discussion. For the rest of the calculations, only the MP2-optimized M·Me_2S(ph) and M·Me_2S(py) structures were taken up.

Table 1 gives all of the geometrical parameters such as the $d_{H\cdots Y}$ (Y= O or S), $R_{N\cdots Y}$, Δr_{NH}, the H-bond angle θ (i.e., ∠NHY), and the angle ψ, that is, the angle between the C_2 axis of the H_2Y (Me_2Y) and the NH···Y bond. It also includes the geometrical parameters for L = H_2S and Me_2O for the sake of comparison as experimentally, their complexes with IND and 3-MI could not be observed. H_2S does not form the N−H···S σ-type HB complexes, but it rather forms the S−H···Φ π-type HB complexes. The results obtained for the S−H···Φ π-type HB complexes are very interesting and will be reported in another communication.[63] Similarly, the experiments could not be done with Me_2O due to the unavailability of the compound.

The deviation from the linearity of HB interaction was the least for the M·H_2O (θ ∼170°) complexes followed by M·Me_2S (θ ∼170°), M·Me_2O (θ ∼165°), and M·H_2S (θ ∼158°) complexes. The increase in the N−H bond length in the M·H_2O complex was almost half of that for the M·Me_2S complex, which is consistent with the observed N−H stretch red shift. However, the increase in the N−H bond length in the M·Me_2O and M·Me_2S complexes was comparable. This suggests that the N−H···Y interaction is not only governed by the identity of the Y atom but also the substituents on the Y atom. In this particular case, the differences in the θ and Δr parameters in the case of the H_2O versus H_2S system diminish when the system changes to Me_2O versus Me_2S. The major difference in the geometry for the "O" acceptor and "S" acceptor was the magnitude of angle ψ. Regardless of the substitution on the S atom, the angle ψ for the N−H···S complexes was 84−90°, whereas for the water complex, it was ∼155°. This was also noted for the O−H···O and O−H···S HB systems previously.[4,5] For the Me_2O complex, however, it was intermediate, namely, 128°.

TABLE 2: Calculated Binding Energy and Different Correction Terms (kcal/mol) for IND·L and 3-MI·L Complexes (L = H_2O, H_2S, Me_2O, and Me_2S)

	indole·L					3-methylindole·L				
energy components	H_2O	H_2S	Me_2O	Me_2S(ph)	Me_2S(py)	H_2O	H_2S	Me_2O	Me_2S(ph)	Me_2S(py)
ΔE_{BE} (kcal/mol)	–6.71	–5.08	–9.62	–9.39	–8.36	–6.57	–5.03	–9.52	–9.40	–8.44
ΔE_{BSSE}	1.25	1.74	2.57	3.64	3.15	1.27	1.77	2.64	3.74	3.29
ΔE_{Relax}	0.07	0.04	0.25	0.26	0.12	0.07	0.04	0.25	0.24	0.11
ΔE_{BE}^{BSSE}	–5.46	–3.34	–7.04	–5.75	–5.21	–5.29	–3.26	–6.88	–5.66	–5.14
ΔZPE	1.22	1.07	0.85	0.84	0.66	1.24	1.07	0.87	0.86	0.70
$\Delta E_{BE}^{BSSE+Relax+ZPE}$	–4.16	–2.22	–5.94	–4.65	–4.43	–3.99	–2.14	–5.76	–4.56	–4.33
ΔE_0^{CBS}	–4.53	–2.74	–6.47	–5.59	---	–4.35	–2.66	–6.29	–5.51	---

The interaction energies for the complexes calculated at the MP2/aug-cc-pVDZ level of theory are provided in Table 2. First row of Table 2 lists the uncorrected binding energy (ΔE_{BE}), which was taken as the difference between the energy of the complex and that of the monomers. Various energy corrections like basis set superposition error (ΔE_{BSSE}), deformation or relaxation energy (ΔE_{Relax}), and zero-point energy correction (ΔZPE) were applied to get the corrected interaction energy ($\Delta E_{BE}^{BSSE+Relax+ZPE}$). According to the NIST computational chemistry comparison and benchmark database,[64] a scaling factor of 0.959 was used to scale the ZPE computed at the MP2/aug-cc-pvDZ level of theory. In Table 2, the subscripts to ΔE indicate the corresponding correction energy term, and the superscripts indicate the energy corrections that were applied. The corrected binding energies of IND·H_2O and 3-MI·H_2O are 4.16 and 3.99 kcal/mol, respectively, which is about 90% of the experimentally determined binding energy.[35,65] The binding energy for the M·Me_2S(ph) complex is ∼0.2 kcal/mol higher than that of the M·Me_2S(py) complex and ∼0.5 kcal/mol greater than that of the M·H_2O complex. To estimate the binding energy more precisely, single-point energy calculation was done at the MP2/aug-cc-pVTZ level of theory for all of the MP2/aug-cc-pvDZ optimized phenyl-oriented complexes. The interaction energies at the complete basis set (CBS) limit for the MP2/aug-cc-pVDZ optimized structures were estimated using the two-point extrapolation formula of Helgaker et al.[42]

$$E^{CBS} \approx \frac{X^3E(X) - (X-1)^3E(X-1)}{X^3 - (X-1)^3} \qquad X = 3 \text{ for the aug-cc-pVTZ basis set} \quad (1)$$

The ZPE and deformation-energy-corrected complete basis set interaction energy (ΔE_0^{CBS}) is provided in the last row of Table 2. The corrected binding energies of IND·H_2O and 3-MI·H_2O are 4.53 and 4.35 kcal/mol, respectively, which is about 97% of the experimentally determined binding energy.[35,65] This indicates that the binding energies estimated at the aforementioned level of computation are acceptable. It is apparent from the values listed in the Table 2 that as the hydrogens in H_2O/H_2S are replaced by the methyl groups, the difference in the binding energies of the corresponding pair of complexes decreases. For instance, the binding energy ratio for the M·H_2O to M·H_2S complex is ∼1.65, whereas that for the M·Me_2O and M·Me_2S complex is ∼1.15. This suggests that the methyl groups must be contributing toward the net interaction energy either by induction forces or dispersion, making the N−H···S HB complexes relatively stronger. A greater binding energy of the M·Me_2S than that of the M·H_2O complex is qualitatively in line with the greater relative red shift of N−H stretches in these complexes. However, quantitatively, this is not commensurate, that is, the red shifts in the case of N−H···S complexes are greater by almost a factor of 2.

5.2. Atoms in Molecules (AIM) Study. The AIM theory proposed by Bader[44−46] was used to obtain greater insight into the N−H···S and N−H···O hydrogen bonds. AIM calculations were done using the ab initio wave functions computed at the MP2 level of theory for the monomers and the complexes. The molecular graphs for IND·Me_2S (Figure 8a and b) and 3-MI·Me_2S (Figure 8c and d) are depicted in Figure 8. It shows the BCPs along the lines joining the NH and S atom, which establishes the existence of the NH···S hydrogen bond between IND (3-MI) and Me_2S. The AIM criteria proposed by Popelier[66−68] that establishes a classical hydrogen bond were applied to the N−H···O and N−H···S hydrogen-bonded complexes. All of the topological parameters for the M·L(ph)-type complex are listed in Table 3. The charge densities and their Lapalcians at the BCPs were 0.0137−0.0292 and 0.0365−0.1154 au, respectively. These values of the electron density and its Laplacian are well within the range specified for the existence of the hydrogen bond in terms of electron density (0.002−0.040 au) and its Laplacian (0.024−0.139 au).[66,67,69] First, the parameters pertaining only to the H_2O and Me_2S will be compared, and later, they will be put in perspective by comparing those for the H_2O with H_2S and Me_2O with Me_2S complexes. The charge density at the NH···S BCP for the M·Me_2S complex was comparable to that for the M·H_2O complex. The Laplacian and the loss of electronic charge on the hydrogen atom were however almost half as much as those for the M·Me_2S complex. The same trend was also observed for the decrease of dipolar polarization of the hydrogen atom. The destabilization of the hydrogen atom was relatively smaller

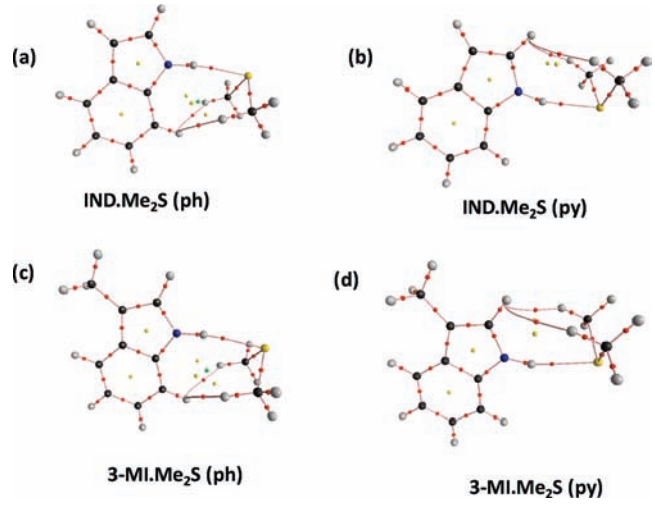

Figure 8. The molecular graph of (a) IND·Me_2S(ph), (b) IND·Me_2S(py), (c)3-MI·Me_2S(ph), and (d)3-MI·Me_2S(py), obtained using MP2/aug-cc-pVDZ wave functions.

TABLE 3: AIM Topological Parameters (au) for IND·L and 3-MI·L Complexes (L = H_2O, H_2S, Me_2O, and Me_2S) Computed Using MP2/aug-cc-pVDZ Wave Functions for the Structures Optimized at the Same Level of Theory

AIM parameters	indole·L				3-methylindole·L			
	H_2O	H_2S	Me_2O	Me_2S	H_2O	H_2S	Me_2O	Me_2S
$\rho_{H\cdots Y}$	0.0222	0.0137	0.0292	0.0218	0.0220	0.0137	0.0292	0.0215
$\nabla^2\rho_{H\cdots Y}$	0.0934	0.0365	0.1092	0.0577	0.0921	0.0366	0.1154	0.0573
Δq_H	0.0650	0.0154	0.1089	0.0345	0.0645	0.0208	0.0767	0.0337
ΔE_H	0.0301	0.0147	0.0354	0.0214	0.0299	0.0144	0.0361	0.0207
$\Delta\lvert M_H\rvert$	–0.0456	–0.0088	–0.0623	–0.0262	–0.0458	–0.0136	–0.0513	–0.0261
Δv_H	–8.6871	–3.0624	–11.0511	–7.6685	–8.6322	–3.6215	–10.5439	–7.6806

TABLE 4: Summary of NBO Analyses with $E^{(2)}_{i\rightarrow j^*}$ in kcal/mol (all other values in au)

NBO parameters	indole complexes				3-methylindole complexes			
	H_2O	H_2S	Me_2O[a]	Me_2S[a]	H_2O	H_2S	Me_2O[a]	Me_2S[a]
Δq(H)	0.0335	0.0133	0.0301	0.0072	0.0334	0.0132	0.0298	0.0070
Δq(Y)	–0.0132	0.0037	–0.0142	0.0000	–0.0123	0.0039	–0.0137	–0.0005
$\delta(n_Y)$	1.9831	1.9803	1.9371, 1.9686	1.9259, 1.9874	1.9833	1.9807	1.9375, 1.9689	1.9269, 1.9875
$\delta(\sigma^*_{N-H})$	0.0273	0.0298	0.0364	0.0461	0.0269	0.0292	0.0354	0.0448
$\varepsilon^{(2)}_{i\rightarrow j}$	14.04	10.36	17.98 (12.32 + 5.66)	19.59 (18.11 + 1.48)	13.84	10.14	17.25 (11.72 + 5.53)	18.89 (17.46 + 1.43)
$\varepsilon^{(0)}_{j^*} - \varepsilon^{(0)}_i$	1.59	1.13	2.74 (1.25 + 1.49)	2.50 (1.05 + 1.45)	1.58	1.14	2.74 (1.25 + 1.49)	2.50 (1.05 + 1.46)
$\langle\varphi^{(0)}_i\lvert\hat{F}^i_{KS}\rvert\varphi^{(0)}_{j^*}\rangle$	0.13	0.10	0.194 (0.112 + 0.082)	0.166 (0.124 + 0.042)	0.13	0.10	0.190 (0.109 + 0.081)	0.163 (0.122 + 0.041)

[a] The values in the parentheses give the individual contribution of the nonbonding orbitals of oxygen and sulfur. The $\delta(n_Y)$ values are for each of the two lone pairs.

for the M·Me_2S complex. The charge densities at the BCPs for both complexes are in line with the computed binding energies. All other parameters suggest that the electrostatic component of the interaction must be greater for the M·H_2O complexes compared to that in the M·Me_2S complexes. Comparison of relative values of the parameters for H_2O versus H_2S and Me_2O versus Me_2S suggests that the M·L complexes involving the sulfur center are weaker than those involving the oxygen center, except that the relative weakness in the dimethyl compounds is much smaller compared to that in the dihydrides. The BCPs were also located in between the methyl C−H of Me_2S and the phenyl and pyrrole C−H of IND and 3-MI. However, the charge densities and their Lapalcians at these BCPs for the M·Me_2S(ph) complex were 0.0071 and 0.0025 au, respectively, and those for the M·Me_2S(py) complex were 0.0041 and 0.0017 au, respectively. These values are too small to suggest any interactions among them and hence can be ignored.

5.3. Natural Bond Orbital (NBO) Analysis. The NBO model has been very useful in explaining the hydrogen bonding in the X-H···Y system as the charge delocalization takes place between the lone pair of the hydrogen-bond acceptor Y and the antibonding σ^*(X−H) orbital of the donor.[48−50,70] The energy lowering caused by the electron delocalization is generally estimated by the second-order perturbation theory. In the NBO formalism, this second-order perturbative energy $E^{(2)}_{i\rightarrow j^*}$ caused by electron density transfer from the lone pair orbital i to the antibonding orbital j* is expressed as

$$E^{(2)}_{i\rightarrow j^*} = -n^{(0)}_i \frac{\langle\Phi^{(0)}_i|\hat{F}_{KS}|\Phi^{(0)}_{j^*}\rangle^2}{\varepsilon^{(0)}_{j^*} - \varepsilon^{(0)}_i} \qquad (2)$$

where $\Phi^{(0)}_i$ and $\Phi^{(0)}_{j^*}$ are the zeroth-order wave functions and $\varepsilon^{(0)}_i$ and $\varepsilon^{(0)}_{j^*}$ are the zeroth-order energies of the lone pair orbital and antibonding orbital, respectively, $n^{(0)}_i$ is the occupancy in the lone pair orbital i, and $\hat{F}_{KS}$ is the Kohn−Sham form of one-electron effective Hamiltonian.[49,50]

Table 4 lists the changes in the atomic charges on H [Δq(H)] and O or S (Δq(Y)) atoms, the occupancy in the lone pair orbital [$\delta(n$Y)] and the antibonding orbital [$\delta(\sigma^*_{N-H})$], and the second-order perturbative interactions in the M·L complexes. The charge reduction on the H atom (increase in the electron density) was larger for the M·H_2O and M·Me_2O complexes than that for their S counterparts, that is, for the M·H_2S and M·Me_2S complexes. The population in the σ^*_{N-H} orbital for the M·H_2O and M·Me_2O complexes was smaller than that for their S counterparts. The $E^{(2)}_{i\rightarrow j^*}$ values (Table 4) for the M·Me_2S complexes than the M·H_2O complexes suggest that there is greater overlap of the lone pair and N−H antibonding orbital in the former complexes. All of these numbers support the greater red shift in the N−H stretch for the M·Me_2S complexes than that for the M·H_2O complexes. For the analogous pairs of M·H_2O and M·H_2S complexes, the $E^{(2)}_{i\rightarrow j^*}$ values suggest that there is a greater overlap of the lone pair (LP) orbital and the N−H antibonding orbital in the N−H···O interaction than that in the N−H···S interaction. However, in the case of M·Me_2O and M·Me_2S complexes, it is other way around, that is, the overlap of the lone pair (LP) orbitals and the N−H antibonding orbital in M·Me_2S complexes is greater than that in the M·Me_2O complexes. The $E^{(2)}_{i\rightarrow j^*}$ values and the shift in the N−H stretch for the M·H_2S and M·H_2O complexes cannot be compared directly as H_2S does not form a N−H···S σ-type hydrogen-bonded complex with indole and 3-MI. Similarly, due to the lack of the experimental data for the M·Me_2O complexes, it is difficult to correlate the $E^{(2)}_{i\rightarrow j^*}$ values with the shift in the N−H stretch. However, the computed values of the red shift in the N−H stretch for the M·Me_2O and M·Me_2S complexes are very similar (the red shifts in the N−H stretch for the IND·Me_2O and IND·Me_2S complexes are 222 and 220 cm^{-1}, respectively, and those for 3-MI·Me_2O and 3-MI·Me_2S are 213 and 212 cm^{-1}, respectively). This is consistent with the similar $E^{(2)}_{i\rightarrow j^*}$ values for the M·Me_2O and M·Me_2S complexes (Table 4).

5.4. Energy Decomposition Analysis. To better understand the nature and the extent of different forces contributing to the intermolecular attraction in these complexes, individual energy components [electrostatic (ES), polarization (PL), and charge transfer (CT)] of the total interaction energy were obtained using the Kitaura and Morokuma (KM),[56] reduced vibrational space

TABLE 5: Various Contributions to the Total Interaction Energy According to the RVS Energy Decomposition Analyses[a]

complex	ΔE_{CT}	ΔE_{ES}	ΔE_{PL}	ΔE_{EX}	ΔE_{BSSE}	ΔE_{MIX}	ΔE_{INT}	ΔE_{INT}^{BSSE}	ΔE_{MP2}^{BSSE}	ΔE_{Corr}	%Corr
					Indole						
H_2O	–1.09	–8.57	–1.35	7.23	–0.23	0.13	–4.14	–3.91	–5.46	–1.55	28.35
H_2S	–0.86	–5.10	–0.73	6.39	–0.30	0.09	–0.69	–0.39	–3.34	–2.95	88.32
Me_2O	–1.89	–11.24	–2.00	12.64	–0.53	0.26	–3.28	–2.75	–7.04	–4.29	60.96
Me_2S	–2.26	–8.44	–1.66	13.42	–0.58	0.24	0.24	0.82	–5.75	–6.57	114.25
					3–Methylindole						
H_2O	–1.07	–8.34	–1.31	7.15	–0.23	0.13	–3.93	–3.70	–5.29	–1.59	30.10
H_2S	–0.84	–5.01	–0.70	6.40	–0.31	0.09	–0.55	–0.24	–3.26	–3.02	92.64
Me_2O	–1.83	–10.95	–1.91	12.50	–0.55	0.25	–2.99	–2.44	–6.88	–4.44	64.52
Me_2S	–2.20	–8.22	–1.60	13.26	–0.59	0.21	0.44	1.03	–5.66	–6.69	118.20

[a] All of the energy components are in kcal/mol. The last column in the table denotes the percentage of contribution of correlation or dispersion interaction to the total interaction energy.

TABLE 6: Summary of Binding Energy, Red Shift in the N−H Stretch ($\Delta\nu_{NH}$), and Band Origin (ΔE_{BO}) for Different Types of N−H···Y Hydrogen Bonded Complexes (N−H···O, N−H···S, and N−H···π) of Indole and 3-Methylindole

			indole complexes			3-methylindole complexes		
ligand	PA (kcal/mol)	α (Å^3)	BE (kcal/mol)	$\Delta\nu_{NH}$ (cm^{-1})	ΔE_{BO} (cm^{-1})	BE (kcal/mol)	$\Delta\nu_{NH}$ (cm^{-1})	ΔE_{BO} (cm^{-1})
H_2O	166.5	1.501	−4.67[a,c]	89	132	−4.49[a,e]	84	233
Me_2S	198.6	7.550	−5.59[b]	158	170	−5.51[b]	154	258
benzene	179.3	6.539	−5.21[a,d]	46	164	−5.07[a,f]	42	252

[a] Experimentally determined binding energy. [b] Computed at the complete basis set limit. [c] Reference 65. [d] Reference 60. [e] Reference 35. [f] Reference 37.

self-consistent field (RVS),[57] and natural energy decomposition analysis (NEDA)[48] procedures. The total interaction energy along with the individual components obtained using the RVS schemes at the HF/aug-cc-pVDZ level are listed in Table 5. The results of KM and NEDA analyses are not shown here, but these two schemes give a similar result as that of the RVS scheme. The correlation energy or the dispersion energy was calculated as the difference between the BSSE-corrected total interaction energy computed at the MP2 level and that computed using the KM, RVS, and NEDA procedures. In the case of M·H_2O, the ES, CT, and PL contributions are large, while for the M·H_2S and M·Me_2S complexes, the dispersion energy was substantially greater than all other energy contributions. For the H_2S complex, it was as large as 88%, whereas for the Me_2S complex without the dispersion energy, the complex is predicted to be unstable. It shows that the N−H···S HB is purely dispersive in nature. In the case of H_2O versus Me_2O complexes, it is noted that with the methyl substitution, the dispersion contribution to the net binding energy increased from 28 to 61%. This indicates that the increase in the binding energy of the Me_2O complex relative to the H_2O complexes must be entirely due to the increase in the dispersion contribution, as pointed out earlier. It is worth comparing the correlation energy obtained for the N−H···S HB systems in this work to that of C−H···Φ systems.[71−74] The magnitude of the correlation energy in the present case is very similar to that in the case of the benzene·$CHCl_3$ complex but much smaller than that in the benzene·CH_4 complex.[74] However, in all of these cases, the correlation energy was the major contributor toward the stability of the complexes.

6. Discussion

In the present context, the experimental data such as the shifts in the S_1-S_0 band origin and the red shifts in the N−H stretching frequency in the case of M·Me_2S complexes suggest that the M acts as the HB donor and the sulfur atom of Me_2S acts as the acceptor. This is consistent with the equilibrium structures computed at the MP2/aug-cc-pVDZ level of theory. Although in the R2PI spectrum only one conformer was observed, it was predicted that in the case of Me_2S, two conformers are possible, as pointed out earlier. The IR spectra in the C−H stretch region were recorded for the monomer as well as the M·H_2O and M·Me_2S complexes to find the signatures of the orientation of methyl groups in the Me_2S complexes, but it did not help. Further, the computed IR spectra for the two conformers did not offer any distinction between them. A similar situation has also been reported for the IND·H_2O complex, where R2PI spectra give evidence for the existence of one conformer[30] while the rotationally resolved ultraviolet spectrum shows a tunneling doublet as a result of the hindered rotation of H_2O about the N−H···O bond.[75] Our data indicated that the phenyl and pyrrole C−H stretches of M·Me_2S complexes were broadened compared to the corresponding monomer C−H stretches. Therefore, we suggest that, as in the case of H_2O, the broadening of the phenyl CH stretches is due to the hindered rotation of Me_2S about the N−H···S bond. The barrier for the rotation should be much smaller in the case of Me_2S due to the bulkiness of the two methyl groups. The methyl C−H stretches of Me_2S at 2925, 2929, and 2975 cm^{-1} were blue shifted up to 6 cm^{-1} compared to the monomer C−H stretches.[62] This blue shift is due to the trans lone pair effect. In the case of a HB complex between a proton donor molecule X−H and the lone pair of a base (Y:) carrying CH_3 groups, the extent of the trans lone pair decreases compared to that in the isolated molecule. This makes the $C-H_{trans}$ bond become stronger in the complex than that in the monomer, which leads to a blue shift in the C−H stretch. This observation was also reported earlier in the matrix-isolated FTIR spectra of the $(CH_3)_2Y\cdots H-X$ type HB complexes, where Y = O, S, and Se atoms.[76−78]

The binding energies for all of the M·L (M= IND, 3-MI, and L = H_2O, H_2S, Me_2O, Me_2S) complexes were computed at the MP2/CBS limit to compare the strength of the N−H···S HB with that of the N−H···O HB (Table 2). The computed binding energies for the M·H_2O complexes are almost 97% of the experimentally determined values.[35,65] In the analogous pairs

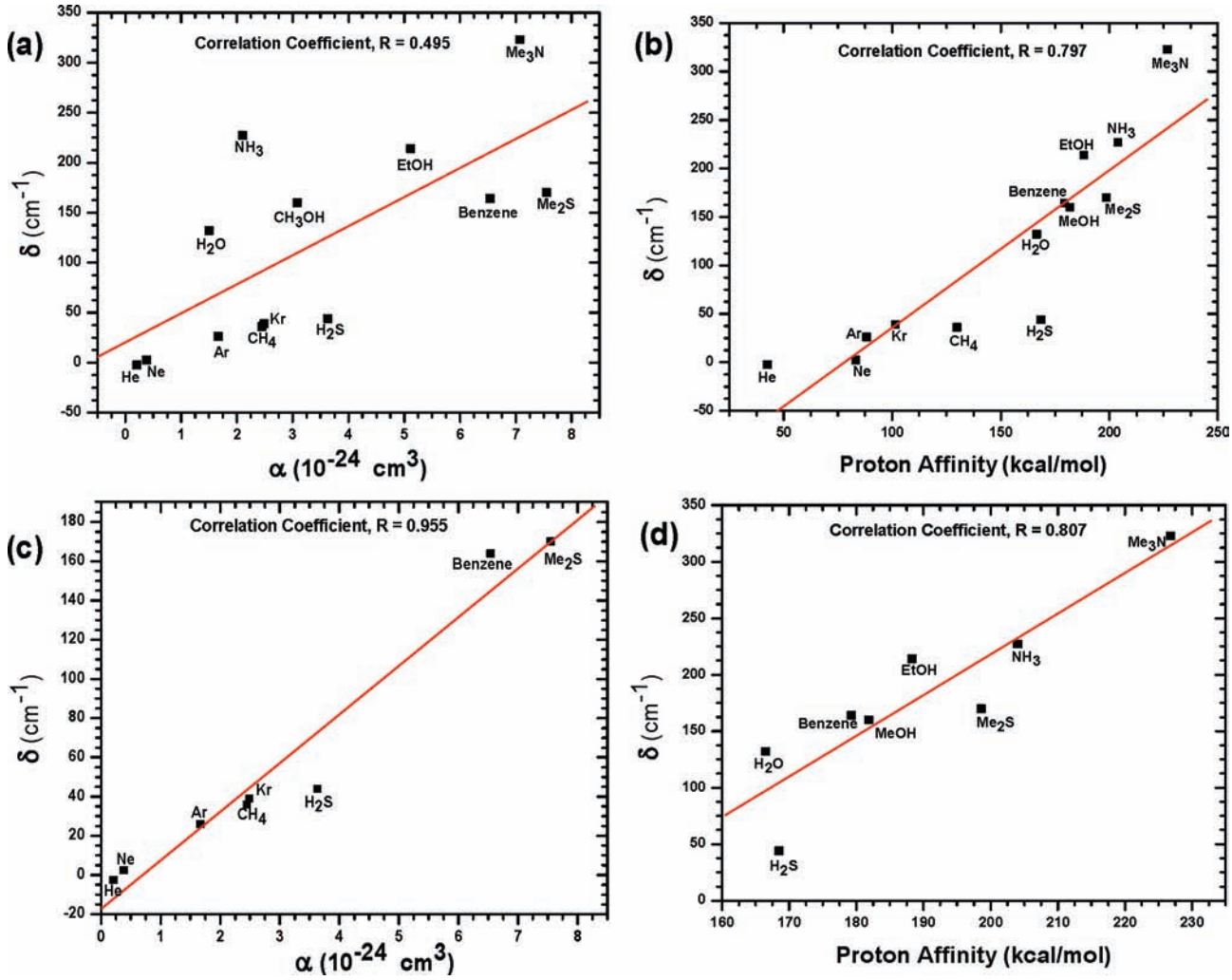

Figure 9. The correlations plot band origin shift (δ) versus polarizabilty (α) and proton affinity (PA) for different types of N−H···Y hydrogen-bonded and van der Waals complexes of indole. (a) The band origin shift (δ) versus polarizabilty (α); (b) the band origin shift (δ) versus proton affinity (PA) plots for all of the complexes; (c) the band origin shift (δ) versus polarizabilty (α) for the van der Waals complexes and M·Me_2S, M·H_2S, and M·benzene; (d) the band origin shift (δ) versus proton affinity (PA) for the N−H···O and N−H···N type HB complexes and M·Me_2S, M·H_2S, and M·benzene.

of complexes, the N−H···S HB is weaker than the N−H···O HB. However, the ratio of the binding energies decreases dramatically from 1:1.65 for the M·H_2S and M·H_2O complex to 1:1.15 for the M·Me_2S and M·Me_2O complexes. This suggests that with the replacement of hydrogens by methyl groups, the strength of the N−H···S HB increases more than that of the N−H···O HB. The binding energies for the M·Me_2S complexes are about 1 kcal/mol more than that of the M·H_2O complexes. This is also reflected in the relative red shift of N−H stretches in the corresponding complexes, even though the magnitude of the red shift is not commensurate with the binding energy. This is in contrast with the observations in the case of *p*-cresol·L (L = H_2O or Me_2S) complexes, that is, the OH···O versus OH···S interaction. The red shift in the O−H stretch of *p*-cresol·L (L = H_2O or Me_2S) complexes was comparable,[4] although the difference in the binding energies of the two complexes was similar to that in the present case, with the *p*-CR·H_2O complex being less stable (4.42 kcal/mol versus 5.31 kcal/mol). This suggests that the interaction between the X−H antibonding orbital and the sulfur lone pair is greater in the case of the N−H···S HB than that in the O−H···S HB.

The band origin shifts, red shifts of N−H stretch, and binding energies of M·Me_2S complexes are compared with those of M·H_2O and M·benzene complexes, and the values are listed in Table 6. The H_2O and benzene complexes were chosen for comparison as the representatives of the σ-type electrostatic HB and π-type dispersive HB complexes, respectively. The band origin shift and the N−H stetching frequency for the M·benzene complexes were also determined in this work. The magnitudes of the band origin shift suggest that the relative stabilization of the S_1 state in the case of M·Me_2S complexes [170 (258) cm^{-1}] are significantly higher than those of M·H_2O complexes [132 (233) cm^{-1}] but comparable with those of benzene complexes [164 (252) cm^{-1}]. The values given in the parentheses correspond to the 3-MI complexes. The comparable band origin shift for M·Me_2S and M·benzene suggests that Me_2S stabilizes the excited state in the same way as benzene does, that is, the Me_2S interaction with IND and 3-MI is dispersive in nature.

There are numerous studies on the hydrogen-bonded complexes of indoles and their derivatives with common solvents such as H_2O, NH_3, and so forth, as well as the van der Waals complexes with the inert gases.[26,27,30,31,33−35,60,79−82] Some efforts have been made to correlate the band origin shift with proton affinity[80] (HB complexes) and polarizabilty[79] (van der Waals complexes). In the HB complexes, electrostatic interaction is the major component of the total interaction energy, while for the van der Waals complexes, the dispersion energy is the major component. Since the computational results suggest that N−H···S

HB is dispersive in nature, our experimental observations are compared with the reported results. In order to ascertain the nature of the N−H···S HB, the band origin shift data for all the known weakly bound IND·L complexes (both HB and van der Waals complexes) were collected and plotted against (a) the proton affinity and (b) the polarizabilty of the ligands. Most of the band origin shift data were taken from Hager et al.'s study,[79,80] and the proton affinity and polarizabilty values were taken from the NIST database.[64,83−86] Figure 9a shows the band origin shift (δ) versus polarizability (α), while Figure 9b shows the band origin shift (δ) versus proton affinity (PA) plots for all of the complexes. The correlation between δ and α or PA is very poor, the correlation coefficients being 0.495 and 0.797, respectively. However, if the entire set is divided into two sets, namely, H-bonded complexes and van der Waals complexes, then it can be shown that the band origin shifts correlate well with PA for the former set and with the polarizability for the later. When the δ values for the M·Me_2S, M·H_2S,[63] and M·benzene are plotted against the polarizability along with those for the van der Waals complexes (Figure 9c), the correlation is excellent with the linear correlation coefficient of 0.955. Conversely, if they are plotted against PA along with those for the H-Bonded complexes (Figure 9d), the correlation is very poor, with a linear correlation coefficient of only 0.807. This suggests that N−H···S HB is different in nature from the conventional N−H···O and N−H···N HB complexes, which is consistent with the energy decomposition analysis.

The relative magnitude of the X−H stretching frequency shift has been invariably used as an indirect measure of the X−H···Y hydrogen bond strength. This shift generally correlates well with the lengthening of the X−H bond, the total interaction energy, as well as the proton affinity of the acceptor. We show here that this basic tenet falls apart in the present case. Table 6 shows that the binding energies of IND and 3-MI complexes with Me_2S, H_2O, and benzene are all comparable, that is, they are within 1 kcal/mol of each other. However, the red shifts of N−H stretch for the three complexes are roughly in the ratio of 4:2:1 (the red shifts in the N−H stretch for the IND·benzene and 3MI·benzene complexes were measured in this work as 46 and 42 cm^{-1}, respectively). For the conventional hydrogen bonds, the X−H red shift is also well correlated with the proton affinity (PA) of the acceptor.[87,88] However, in the present case this is not true. The PA ratio of Me_2S, H_2O, and benzene is ∼1.2:1.0:1.1, that is, they are comparable. Therefore, it must be highlighted here that the IR shifts are inconsistent with both the binding energy and the acid−base formalism of the HB interactions. This is perhaps due to the fact that the acid−base formalism in the context of hydrogen bonding holds well when the electrostatic energy component is the major contributor to the total binding energy. This conjuncture is supported by the energy decomposition analysis (Table 5). The analysis shows that sum of the electrostatic component and charge-transfer energy component for the M·Me_2S complexes was greater than that for the M·H_2O complexes, which is responsible for the larger red shift in the N−H stretch in the former. However, the large repulsive exchange energy component for the M·Me_2S complexes completely cancels the net attractive interaction. Therefore, the overall stabilization of the M·Me_2S complexes comes almost entirely from the dispersive interaction.

7. Conclusions

The nature of N−H···S hydrogen bonding was studied between the two model compounds of the amino acids, namely, indole and 3-methylindole for tryptophan and dimethyl sulfide for methionine. The N−H···S hydrogen-bonded complexes were characterized by using different experimental techniques like REMPI, FDIRS, and RIDIRS and various computational methods. The red shifts in the band origins and N−H stretches for the M·Me_2S complexes were larger compared to those for the M·H_2O complexes. The most striking feature of this study is that the red shift in the N−H stretch for the N−H···S hydrogen-bonded complexes (M·Me_2S) were almost two times that for the N−H···O HB in M·H_2O complexes, although the ab intio results show that the binding energy for the M·Me_2S complexes is only marginally higher than that for the M·H_2O complex, that is, by about 1 kcal/mol in both the cases. This is quite different from the behavior observed in the O−H···S (*p*-CR·Me_2S) hydrogen-bonded complex, where the red shift in the O−H stretch is almost identical for both the O−H···S (*p*-CR·Me_2S) and O−H···O (*p*-CR·H_2O) HB complexes. The band origin shifts of the M·Me_2S give very good correlation with the polarizabilty rather than the proton affinity, which indicates that N−H···S HB is different from the conventional type of HB complex.

In all of the N−H···S HB complexes, the correlation (or dispersion) energy component has significant contribution to the total binding energy. A higher dispersion contribution to the stabilization energy and greater red shifts of N−H stretch in the N−H···S HB complexes relative to those of N−H···O HB complexes indicates that the total stabilization energy is dominated by the dispersion forces, whereas the N−H red shifts are governed by the electrostatic component. On the basis of a large red shift in the NH stretching frequency of the HB donor, the high correlation energy contribution, and good correlation of the band origin shift with the ploraizability in the N−H···S HB systems, it is inferred that N−H···S HB shows the characteristic signatures of both the "σ-type" and the C−H···Φ or N−H···Φ "π-type" HB.

References and Notes

(1) Latimer, W. M.; Rodebush, W. H. *J. Am. Chem. Soc.* **1920**, *42*, 1419.
(2) Buckingham, A. D.; Del Bene, J. E.; McDowell, S. A. C. *Chem. Phys. Lett.* **2008**, *463*, 1.
(3) Sennikov, P. G. *J. Phys. Chem.* **1994**, *98*, 4973.
(4) Biswal, H. S.; Chakraborty, S.; Wategaonkar, S. *J. Chem. Phys.* **2008**, *129*, 184311.
(5) Biswal, H. S.; Shirhatti, P. R.; Wategaonkar, S. *J. Phys. Chem. A* **2009**, *113*, 5633.
(6) Nangia, A.; Desiraju, G. R. *J. Mol. Struct.* **1999**, 65.
(7) Poulos, T. L.; Finzel, B. C.; Howard, A. J. *J. Mol. Biol.* **1987**, *195*, 687.
(8) Cuppvickery, J. R.; Poulos, T. L. *Nat. Struct. Biol.* **1995**, *2*, 144.
(9) Crane, B. R.; Arvai, A. S.; Gachhui, R.; Wu, C. Q.; Ghosh, D. K.; Getzoff, E. D.; Stuehr, D. J.; Tainer, J. A. *Science* **1997**, *278*, 425.
(10) Ueyama, N.; Nishikawa, N.; Yamada, Y.; Okamura, T.; Nakamura, A. *J. Am. Chem. Soc.* **1996**, *118*, 12826.
(11) Ueyama, N.; Nishikawa, N.; Yamada, Y.; Okamura, T.; Oka, S.; Sakurai, H.; Nakamura, A. *Inorg. Chem.* **1998**, *37*, 2415.
(12) Suzuki, N.; Higuchi, T.; Urano, Y.; Kikuchi, K.; Uekusa, H.; Ohashi, Y.; Uchida, T.; Kitagawa, T.; Nagano, T. *J. Am. Chem. Soc.* **1999**, *121*, 11571.
(13) Chakrabarti, P.; Bhattacharyya, R. *Prog. Biophys. Mol. Biol.* **2007**, *95*, 83.
(14) Francois, S.; Rohmer, M. M.; Benard, M.; Moreland, A. C.; Rauchfuss, T. B. *J. Am. Chem. Soc.* **2000**, *122*, 12743.
(15) Krepps, M. K.; Parkin, S.; Atwood, D. A. *Cryst. Growth Des.* **2001**, *1*, 291.
(16) Lynch, D. E.; McClenaghan, I.; Light, M. E.; Coles, S. J. *Cryst. Eng.* **2002**, *5*, 79.
(17) Sundaresan, C. N.; Dixit, S.; Venugopalan, P. *J. Mol. Struct.* **2004**, *693*, 205.
(18) Muthu, S.; Vittal, J. J. *Cryst. Growth Des.* **2004**, *4*, 1181.
(19) Creed, D. *Photochem. Photobiol.* **1984**, *39*, 537.
(20) Strickla, Eh.; Horwitz, J.; Billups, C. *Biochem.* **1970**, *9*, 4914.

(21) Ballew, R. M.; Sabelko, J.; Gruebele, M. *Proc. Natl. Acad. Sci. U.S.A.* **1996**, *93*, 5759.
(22) Yuan, T.; Weljie, A. M.; Vogel, H. *J. Biochem.* **1998**, *37*, 3187.
(23) Desfrancois, C.; Carles, S.; Schermann, J. P. *Chem. Rev.* **2000**, *100*, 3943.
(24) Park, S. T.; Gahmann, A.; He, Y.; Feenstra, J. S.; Zewail, A. H. *Angew. Chem., Int. Ed.* **2008**, *47*, 9496.
(25) Meyer, E. A.; Castellano, R. K.; Diederich, F. *Angew. Chem., Int. Ed.* **2003**, *42*, 1210.
(26) Montoro, T.; Jouvet, C.; Lopez-Campillo, A.; Soep, B. *J. Phys. Chem.* **1983**, *87*, 3582.
(27) Nibu, Y.; Abe, H.; Mikami, N.; Ito, M. *J. Phys. Chem.* **1983**, *87*, 3898.
(28) Cable, J. R. *J. Chem. Phys.* **1990**, *92*, 1627.
(29) Demmer, D. R.; Leach, G. W.; Wallace, S. C. *J. Phys. Chem.* **1994**, *98*, 12834.
(30) Carney, J. R.; Zwier, T. S. *J. Phys. Chem. A* **1999**, *103*, 9943.
(31) Short, K. W.; Callis, P. R. *J. Chem. Phys.* **2000**, *113*, 5235.
(32) Sobolewski, A. L.; Domcke, W.; Dedonder-Lardeux, C.; Jouvet, C. *Phys. Chem. Chem. Phys.* **2002**, *4*, 1093.
(33) Dian, B. C.; Longarte, A.; Zwier, T. S. *J. Chem. Phys.* **2003**, *118*, 2696.
(34) Braun, J.; Neusser, H. J.; Hobza, P. *J. Phys. Chem. A* **2003**, *107*, 3918.
(35) Georgiev, S.; Neusser, H. J. *Chem. Phys. Lett.* **2004**, *389*, 24.
(36) Somers, K. R. F.; Ceulemans, A. *J. Phys. Chem. A* **2004**, *108*, 7577.
(37) Georgiev, S.; Neusser, H. J. *J. Electron Spectrosc. Relat. Phenom.* **2005**, *142*, 207.
(38) David, O.; Dedonder-Lardeux, C.; Jouvet, C.; Sobolewski, A. L. *J. Phys. Chem. A* **2006**, *110*, 9383.
(39) Sukhodola, A. A. *J. Appl. Spectrosc.* **2008**, *75*, 527.
(40) Meenakshi, P. S.; Biswas, N.; Wategaonkar, S. *J. Chem. Phys.* **2002**, *117*, 11146.
(41) Frisch, M. J.; Trucks, G. W.; Schlegel, H. B.; Scuseria, G. E.; Robb, M. A.; Cheeseman, J. R.; Montgomery, J. A., Jr.; Vreven, T.; Kudin, K. N.; Burant, J. C.; Millam, J. M.; Iyengar, S. S.; Tomasi, J.; Barone, V.; Mennucci, B.; Cossi, M.; Scalmani, G.; Rega, N.; Petersson, G. A.; Nakatsuji, H.; Hada, M.; Ehara, M.; Toyota, K.; Fukuda, R.; Hasegawa, J.; Ishida, M.; Nakajima, T.; Honda, Y.; Kitao, O.; Nakai, H.; Klene, M.; Li, X.; Knox, J. E.; Hratchian, H. P.; Cross, J. B.; Bakken, V.; Adamo, C.; Jaramillo, J.; Gomperts, R.; Stratmann, R. E.; Yazyev, O.; Austin, A. J.; Cammi, R.; Pomelli, C.; Ochterski, J. W.; Ayala, P. Y.; Morokuma, K.; Voth, G. A.; Salvador, P.; Dannenberg, J. J.; Zakrzewski, V. G.; Dapprich, S.; Daniels, A. D.; Strain, M. C.; Farkas, O.; Malick, D. K.; Rabuck, A. D.; Raghavachari, K.; Foresman, J. B.; Ortiz, J. V.; Cui, Q.; Baboul, A. G.; Clifford, S.; Cioslowski, J.; Stefanov, B. B.; Liu, G.; Liashenko, A.; Piskorz, P.; Komaromi, I.; Martin, R. L.; Fox, D. J.; Keith, T.; Al-Laham, M. A.; Peng, C. Y.; Nanayakkara, A.; Challacombe, M.; Gill, P. M. W.; Johnson, B.; Chen, W.; Wong, M. W.; Gonzalez, C.; Pople, J. A. *Gaussian 03*, revision D.1; Gaussian, Inc.: Wallingford, CT, 2005.
(42) Helgaker, T.; Klopper, W.; Koch, H.; Noga, J. *J. Chem. Phys.* **1997**, *106*, 9639.
(43) Mercier, S. R.; Boyarkin, O. V.; Kamariotis, A.; Guglielmi, M.; Tavernelli, I.; Cascella, M.; Rothlisberger, U.; Rizzo, T. R. *J. Am. Chem. Soc.* **2006**, *128*, 16938.
(44) Bader, R. F. W. *Atoms in Molecules: A Quantum Theory*; Clarendon Press: Oxford, U.K., 1990.
(45) Bader, R. F. W. *Chem. Rev.* **1991**, *91*, 893.
(46) Bader, R. F. W. In *Encyclopedia of Computational Chemistry*; Schleyer, P. v. R., Allinger, N. L., Gasteiger, T., Clark, J., Kollman, P. A., Schaefer, H. F. S., III, Schreiner, P. R., Eds.; John Wiley & Sons: Chichester, U.K., 1998; Vol. 1; p 64.
(47) Short, K. W.; Callis, P. R. *Chem. Phys.* **2002**, *283*, 269.
(48) Weinhold, F. In *Encyclopedia of Computational Chemistry*; Schleyer, P. v. R., Allinger, N. L., Gasteiger, T., Clark, J., Kollman, P. A., Schaefer, H. F. S., III, Schreiner, P. R., Eds.; John Wiley & Sons: Chichester, U.K., 1998; Vol. 3; p 1792.
(49) Weinhold, F.; Landis, C. R. *Chem. Educ. Res. Pract. Eur.* **2001**, *2*, 91.
(50) Weinhold, F.; Landis, C. R. *Valency and Bonding: A Natural Bond Orbital Donor-Acceptor Perspective*; Cambridge University Press: New York, 2005.
(51) *NBO 5.0*; Glendening, J., Badenhoop, K., Reed, A. E., Carpenter, J. E., Bohmann, J. A., Morales, C. M., Weinhold, F., Eds.; Theoretical Chemistry Institute, University of Wisconsin: Madison, WI, 2001.
(52) Chalasinski, G.; Szczesniak, M. M. *Chem. Rev.* **2000**, *100*, 4227.
(53) Glendening, E. D.; Streitwieser, A. *J. Chem. Phys.* **1994**, *100*, 2900.
(54) Glendening, E. D. *J. Am. Chem. Soc.* **1996**, *118*, 2473.
(55) Schenter, G. K.; Glendening, E. D. *J. Phys. Chem.* **1996**, *100*, 17152.
(56) Kitaura, K.; Morokuma, K. *Int. J. Quantum Chem.* **1976**, *10*, 325.
(57) Stevens, W. J.; Fink, W. H. *Chem. Phys. Lett.* **1987**, *139*, 15.
(58) Chen, W.; Gordon, M. S. *J. Phys. Chem.* **1996**, *100*, 14316.
(59) Schmidt, M. W.; Baldridge, K. K.; Boatz, J. A.; Elbert, S. T.; Gordon, M. S.; Jensen, J. H.; Koseki, S.; Matsunaga, N.; Nguyen, K. A.; Su, S. J.; Windus, T. L.; Dupuis, M.; Montgomery, J. A. *J. Comput. Chem.* **1993**, *14*, 1347.
(60) Braun, J. E.; Grebner, T. L.; Neusser, H. J. *J. Phys. Chem. A* **1998**, *102*, 3273.
(61) Carney, J. R.; Hagemeister, F. C.; Zwier, T. S. *J. Chem. Phys.* **1998**, *108*, 3379.
(62) Ellwood, J. A.; Steele, D.; Gerrard, D. *Spectrochim. Acta, Part A* **1994**, *50*, 913.
(63) H_2S forms an S−H···Φ π-type hydrogen-bonded complex with indole and 3-methylindole; to be published soon.
(64) NIST Computational Chemistry Comparison and Benchmark DataBase; NIST: Gaithersburg, MD, http://cccbdb.nist.gov.
(65) Braun, J. E.; Mehnert, T.; Neusser, H. J. *Int. J. Mass Spectrom.* **2000**, *203*, 1.
(66) Koch, U.; Popelier, P. L. A. *J. Phys. Chem.* **1995**, *99*, 9747.
(67) Popelier, P. L. A. *J. Phys. Chem.* **1998**, *102*, 1873.
(68) Popelier, P. *Atoms In Molecules, An Introduction*; Prentice Hall: Englewood Cliffs, NJ, 2000.
(69) Grabowski, S. J. *J. Phys. Org. Chem.* **2004**, *17*, 18.
(70) Reed, A. E.; Curtiss, L. A.; Weinhold, F. *Chem. Rev.* **1988**, *88*, 899.
(71) Tsuzuki, S.; Honda, K.; Uchimaru, T.; Mikami, M.; Tanabe, K. *J. Am. Chem. Soc.* **2000**, *122*, 11450.
(72) Tsuzuki, S.; Honda, K.; Uchimaru, T.; Mikami, M.; Tanabe, K. *J. Phys. Chem. A* **2002**, *106*, 4423.
(73) Tsuzuki, S.; Uchimaru, T. *Curr. Org. Chem.* **2006**, *10*, 745.
(74) Fujii, A.; Shibasaki, K.; Kazama, T.; Itaya, R.; Mikami, N.; Tsuzuki, S. *Phys. Chem. Chem. Phys.* **2008**, *10*, 2836.
(75) Korter, T. M.; Pratt, D. W.; Kupper, J. *J. Phys. Chem. A* **1998**, *102*, 7211.
(76) McKean, D. C. *Chem. Soc. Rev.* **1978**, *7*, 399.
(77) Vanderheyden, L.; Maes, G.; Zeegershuyskens, T. *J. Mol. Struct.* **1984**, *114*, 165.
(78) Maes, G. *J. Mol. Spectrosc.* **1985**, *114*, 289.
(79) Hager, J.; Wallace, S. C. *J. Phys. Chem.* **1983**, *87*, 2121.
(80) Hager, J.; Wallace, S. C. *J. Phys. Chem.* **1984**, *88*, 5513.
(81) Tubergen, M. J.; Levy, D. H. *J. Phys. Chem.* **1991**, *95*, 2175.
(82) Arnold, S.; Sulkes, M. *J. Phys. Chem.* **1992**, *96*, 4768.
(83) Hunter, E. P. L.; Lias, S. G. *J. Phys. Chem. Ref. Data* **1998**, *27*, 413.
(84) Alms, G. R.; Burnham, A. K.; Flygare, W. H. *J. Chem. Phys.* **1975**, *63*, 3321.
(85) Rice, J. E.; Taylor, P. R.; Lee, T. J.; Almlof, J. *J. Chem. Phys.* **1991**, *94*, 4972.
(86) Christiansen, O.; Hattig, C.; Jorgensen, P. *Spectrochim. Acta, Part A* **1999**, *55*, 509.
(87) Iwasaki, A.; Fujii, A.; Watanabe, T.; Ebata, T.; Mikami, N. *J. Phys. Chem.* **1996**, *100*, 16053.
(88) Fujii, A.; Ebata, T.; Mikami, N. *J. Phys. Chem. A* **2002**, *106*, 8554.

JP907658W